Delineating pathological pathways in a chemically-induced mouse model of Gaucher disease

Ayelet Vardi[1,#], Hila Zigdon[1,#], Anna Meshcheriakova[1], Andrés D Klein[1,@], Chen Yaacobi[1], Raya Eilam[2], Brandon M. Kenwood[3], Ahad A. Rahim[4], Giulia Massaro[4], Alfred H. Merrill Jr.[3], Einat B. Vitner[1,^] and Anthony H. Futerman[1,*]

[1]Departments of Biological Chemistry and [2]Veterinary Resources, Weizmann Institute of Science, Rehovot, Israel; [3]School of Biology and Petit Institute for Bioengineering and Bioscience, Georgia Institute of Technology, Atlanta, GA, USA; [4]Deparment of Pharmacology, School of Pharmacy, University College London, London, UK;

[#] Both authors contributed equally to this study

[@] Current address: Telethon Institute of Genetics and Medicine, Pozzuoli, Italy

[^] Current address: Department of Infectious Diseases, Israel Institute for Biological Research, Ness-Ziona, Israel

*Correspondence to A.H. Futerman, Department of Biological Chemistry, Weizmann Institute of Science, Rehovot 76100, Israel. Fax, +(972)-8-9344112; Tel, +(972)-8-9342704; e-mail, tony.futerman@weizmann.ac.il

Conflict of interest: The authors have no conflicts of interest to declare.

This article has been accepted for publication and undergone full peer review but has not been through the copyediting, typesetting, pagination and proofreading process, which may lead to differences between this version and the Version of Record. Please cite this article as doi: 10.1002/path.4751

Abstract

Great interest has been shown in understanding the pathology of Gaucher disease (GD), due to the recently discovered genetic relationship with Parkinson's disease. For such studies, suitable animal models of GD are required. Chemical induction of GD by inhibition of acid β-glucosidase (GCase) using the irreversible inhibitor, conduritol B-epoxide (CBE), is particularly attractive, although few systematic studies examining the effect of CBE on development of symptoms associated with neurological forms of GD have been performed. We now demonstrate a correlation between the amount of CBE injected into mice and levels of accumulation of the GD substrates, glucosylceramide and glucosylsphingosine, and show that disease pathology, indicated by altered levels of pathological markers, depends on both levels of accumulated lipids and the time at which their accumulation begins. Gene array analysis shows a remarkable similarity in the gene expression profiles of CBE-treated mice and a genetic GD mouse model, the *Gba*$^{flox/flox}$;nestin-Cre mouse, with 120 of the 144 genes up-regulated in CBE-treated mice also up-regulated in *Gba*$^{flox/flox}$;nestin-Cre mice. We also demonstrate that various aspects of neuropathology and some behavioral abnormalities can be arrested upon cessation of CBE treatment during a specific time window. Together, our data demonstrate that injection of mice with CBE provides a rapid and relatively easy way to induce symptoms typical of neuronal forms of GD. This is particularly useful when examining the role of specific biochemical pathways in GD pathology, since CBE can be injected into mice defective in components of putative pathological pathways, alleviating the need for time-consuming crossing of mice.

Key words: Gaucher disease, Parkinson's disease, acid β-glucosidase, glucosylceramide, glucosylsphingosine, neuropathology, neuroinflammation.

Introduction

Gaucher disease (GD), one of the most common lysosomal storage disorders (LSDs) (1), is caused by mutations in *GBA1* (2), the gene encoding the lysosomal hydrolase, acid β-glucosidase (GCase). The resulting GCase deficiency causes accumulation of the glycosphingolipids (GSLs), glucosylceramide (GlcCer) and its deacylated form, glucosylsphingosine (GlcSph), within the lysosomes of macrophages and other cells. GD is classified into three types, with all three displaying hepatosplenomegaly, anemia, thrombocytopenia, leukopenia and bone involvement (3, 4), with the neurological forms (nGD), type 2 (acute) and type 3 (chronic), displaying central nervous system (CNS) involvement in addition to systemic disease. The recently-discovered genetic association between mutations in *GBA1* and Parkinson's disease (5) has significantly enhanced the visibility of GD and nGD research, and renders characterization of nGD animal models of critical importance. Currently, two kinds of nGD mice are available, namely genetic models (6-14) and a chemically-induced model. In $Gba^{flox/flox}$;nestin-Cre mice (15), GCase deficiency is restricted to neurons and macroglia, with normal GCase activity in microglia, whereas K14-lnl/lnl mice develop a more rapidly-progressing neurological disease (15). Both of these mice have proven useful in nGD research, but their limited life-spans and the severity of their symptoms restrict their usefulness. Injection with the irreversible GCase inhibitor, conduritol B-epoxide (CBE) (16), has also proved of great use, particularly since CBE crosses the blood brain barrier (BBB) (17). While CBE has been widely used, and increasingly so because of attention paid to the GD/Parkinson's disease enigma, its use has been somewhat erratic, inasmuch as different laboratories inject with different doses, at different ages and using different species of mice (Table 1).

To determine the appropriateness of CBE as a means to induce GD, and to fully characterize its action, we now systematically inject different amounts of CBE into mice of

different ages, and demonstrate that pathology is very similar to the two genetic models discussed above. Moreover, characterization of mice injected with CBE provides novel mechanistic insight into disease pathology. We suggest that the CBE model, even though it has inherent limitations, as do all mouse models, is nevertheless a useful and rapid means to induce nGD. In addition, we demonstrate that cessation of CBE treatment can arrest some but not all symptoms of nGD, and discuss how this experimental approach could be used to test the efficacy of potential therapies.

Materials and methods

Mice

From postnatal days 8 or 15, C57BL/6 mice (Harlan Laboratories, Israel) were injected intra-peritoneally (IP) daily with 25, 37.5, 50 or 100 mg CBE (Calbiochem Millipore, Darmstadt, Germany) per kg body weight, or with PBS. *Gba*$^{flox/flox}$ mice were crossed with *Gba*$^{flox/WT}$;nestin-Cre mice to generate *Gba*$^{flox/flox}$;nestin-Cre mice and *Gba*$^{flox/WT}$;nestin-Cre mice, which served as healthy controls. Genotyping was performed by polymerase chain reaction. Mice with a mixed genetic background (C57BL6/J and CBA with further back-crossings with C57BL6/J; Jackson Laboratories, USA) were also injected with CBE; this mouse expresses Thy1-YFP-H in some cortical neurons (18). Mice were maintained in the experimental animal center of the Weizmann Institute of Science. All animal experiments were approved by the Weizmann Institute Institutional Animal Care and Use Committee. The use of K14-lnl/lnl mice is documented in the Supporting Information.

GCase activity assays and sphingolipid analysis

GCase activity assay was performed as described, as was sphingolipid analysis by liquid chromatography electrospray ionization tandem mass spectrometry (LC-ESI-MS/MS) (8); for more details, see the Supporting Information.

RNA extraction and quantitative PCR

RNA extraction and quantitative PCR were performed as described (9). A detailed description, along with the primers used for PCR, is given in the Supporting Information.

Immunohistochemistry

MAC2 staining was performed as described (7) and a detailed description, along with the methods used for GFAP and fluoro-Jade C staining, is given in the Supporting Information.

Microarray analysis

Starting from postnatal day 8, C57BL/6 mice were injected IP daily for 10 days with 25 mg CBE per kg body weight or with PBS. Microarray analysis was performed as documented in the Supporting Information.

Behavioral experiments

Behavioral tests were performed (23, 24) as documented in the Supporting Information.

Results

The effect of different concentrations of CBE on nGD pathology and comparison to *Gba*$^{flox/flox}$;nestin-Cre mice

While previous studies have used a wide variety of CBE concentrations, ranging from 7.5 to 300 mg/kg body weight (Table 1), little effort has been made to systematically compare the effects of CBE on development of nGD symptoms, and to determine how this correlates with levels of GlcCer and GlcSph accumulation. We injected C57BL/6 mice every day, starting on day 8, with different concentrations of CBE and measured the body weights of the mice and their life-spans. As might be predicted, the highest CBE concentration (100 mg/kg body weight) had the most dramatic effect, with C57BL/6 mice beginning to lose weight by

16 days of age and most not surviving beyond 20 days of age (Fig. 1A). Mice injected with 50 mg/kg also displayed rapid weight loss, again starting on day 16, but survived longer, dying between 24 and 36 days of age. Lower doses had a less severe effect, but even the lowest (25 mg/kg) led to death by 45 days of age, with a relatively high variability between individual mice (Fig. 1A). Interestingly, mice injected with 100 mg/kg CBE starting on day 15 lived considerably longer than mice injected from day 8 (Fig. 1B) and showed less severe symptoms, suggesting a hitherto unappreciated effect of the age of the mice on the ability of CBE to induce nGD symptoms.

GCase activity was measured *in vitro* in brain samples from CBE-treated mice. GCase activity was reduced by >90-95%, irrespective of the concentration of CBE injected (data not shown). We next measured levels of GlcCer and GlcSph accumulation using a new LC-ESI-MS/MS method (Duan et al., submitted for publication) that allows separation of hexosylsphingosine species into GlcSph and galactosylsphingosine (GalSph). GlcCer and GlcSph levels increased linearly with CBE concentration (Fig. 1C; r^2 of 0.95 and 0.96, respectively). It should be noted that GlcSph levels in control mice (~0.2 ± 0.1 pmol/mg tissue) were close to the limit of detection, whereas GlcCer levels were significantly higher in control mice (~35 ± 5.7 pmol/mg tissue). A correlation was also observed between the average day of death of the mice and GlcCer levels (r^2 = 0.91), and to a somewhat lower extent to GlcSph levels (r^2=0.83). Levels of GlcCer (338 ± 74 pmol/mg tissue) and GlcSph (28 ± 12 pmol/mg tissue) in 21-day old *Gba*$^{flox/flox}$;nestin-Cre mouse were similar to levels observed in mice injected with >50 mg/kg body weight CBE; since GCase activity is only defective in cells of neuronal origin in *Gba*$^{flox/flox}$;nestin-Cre mice, this suggests even higher levels of accumulation in cells defective in GCase. Note that no significant changes were observed in either galactosylceramide (GalCer) or GalSph levels (Fig. 1C).

To further dissect changes in sphingolipid levels, the *N*-acyl chain composition of

GlcCer was analyzed. Normal brain tissue contains particularly high levels of C18- and C24:1-sphingolipids (25), and as expected, this was the case in C57BL/6 mice injected with PBS (Fig. 1D and Table S2). However, the higher the CBE dose, the greater the increase in the proportion of C18:0-GlcCer and C18:1-GlcCer versus total GlcCer (C18:0-GlcCer was 85% of total GlcCer upon injection of 100 mg CBE/kg body weight, compared to 68% using 25 mg CBE/kg body weight), which were elevated at the expense of GlcCer with longer acyl chains. Likewise, the acyl chain composition of *Gba*$^{flox/flox}$;nestin-Cre mouse was biased towards C18-GlcCer; similar results have been obtained in other nGD mouse models (26). Since C18-GlcCer is most abundant in neurons (27), this data supports our previous finding using electron microscopy that significant levels of GlcCer accumulate in nestin-expressing cells (*i.e.* neurons and astroglia) in nGD mouse brain (8). Finally, we compared GlcCer levels in mice injected for 10 days with 100 mg/kg body weight CBE starting on day 8 *vs.* day 15. Significantly lower levels of both of these lipids were detected in the latter (Fig. 1E), consistent with data showing that CBE is less effective in generating nGD symptoms when injected into slightly older mice (Fig. 1A, B).

Biochemical and genetic profile of CBE treated mice

We have recently shown changes in levels of a number of inflammatory and other gene transcripts in *Gba*$^{flox/flox}$;nestin-Cre mice ((6, 7, 28) and unpublished data), and we now compare these changes with those observed in mice injected with CBE. The trend of the changes in gene expression was similar, although changes occurred to a different extent (Fig. 2A). Expression of two neuronal genes (*Grin2b* and *Kctd16*) decreased to a similar extent in CBE and *Gba*$^{flox/flox}$;nestin-Cre mice, presumably due to neuronal loss, whereas levels of inflammatory genes (such as *Gfap*, *Ccl3* and *Ccl2*) increased as the CBE concentration increased and reached levels similar to those detected in the *Gba*$^{flox/flox}$;nestin-Cre mouse (Fig. 2A). Members of the *RipK* pathway (*Rip1*, *Rip3* and *Pkr*) (6) were elevated to a somewhat

lower extent in CBE-injected mice compared to *Gba*$^{flox/flox}$;nestin-Cre mice, as were *Ccl5* and *Irf7*, and the expression levels of some of these genes showed little or no correlation to levels of lipid accumulation. Levels of *Gfap*, a marker of astrogliosis, and of *Gpnmb*, a protein recently shown to act as a genuine nGD marker (28), correlated with CBE levels. The expression of most of the genes correlated linearly with changes in GlcCer and/or GlcSph levels, *e.g. Ccl5*, *Cd68* and *Ccl2*, a macrophage-derived cytokine that was suggested to be elevated by GlcCer (10, 29).

We next performed a gene array study using the cortex of C57BL/6 mice injected with 25 mg/kg CBE from days 8 to 18. Table 3 indicates the top 10 up- and down-regulated genes in the array. Next, we compared genes altered in mice injected with CBE (fold-change ≥1.5, *p* value ≤0.05) with those altered in the ventral posteromedial/posterolateral (VPM/VPL) region of the thalamus of 14-day old *Gba*$^{flox/flox}$;nestin-Cre mice (fold-change ≥2, *p* value ≤0.05; Vitner et al., submitted for publication). The number of genes increased in *Gba*$^{flox/flox}$;nestin-Cre mice was ~4 fold higher than in CBE-treated mice (Fig. 2B), presumably because the disease in the CBE model is less severe at this stage; however, striking similarities were found. Thus, 144 genes were up-regulated in CBE-treated mice, of which 120 were also up-regulated in *Gba*$^{flox/flox}$;nestin-Cre mice. Common up-regulated genes were next subjected to pathway analysis. Among these genes, inflammatory pathways such as complement system and the interferon signaling pathway, were highly enriched (Fig. 2C). Notably, inflammatory genes were up-regulated in both models even though, as opposed to the CBE model, the *Gba*$^{flox/flox}$;nestin-Cre mouse does not accumulate GlcCer and GlcSph in microglia. Interestingly, many of the genes that were up-regulated only in the *Gba*$^{flox/flox}$;nestin-Cre mouse belong to the same pathways as altered in mice injected with CBE. However, there were several pathways that were enriched only in the *Gba*$^{flox/flox}$;nestin-Cre mice, including death receptor signaling (Fig. S1), which may be related to neuronal loss observed in the

Gba$^{flox/flox}$;nestin-Cre at day 14 compared to the little neuronal loss observed in mice injected with CBE at day 18.

We next examined the regional selectivity of pathological changes in CBE-treated mice compared to *Gba*$^{flox/flox}$;nestin-Cre mice. Mice were injected with 37.5 mg/kg body weight CBE starting on post-natal day 8, followed by examination of MAC2 immunoreactivity at various times (7). A low level of MAC2 immunoreactivity was observed on day 14 (Fig. 3A), but by day 18, microglia activation was evident in many brain areas, though predominantly in the brain stem and in cortical layer V. By 25 days, MAC2 immunoreactivity was widespread. Interestingly, the brain stem displayed much stronger MAC2 immunoreactivity in CBE-treated mice than *Gba*$^{flox/flox}$;nestin-Cre mice. As in *Gba*$^{flox/flox}$;nestin-Cre mice, a number of brain areas did not show neuropathology (Table 2).

We also analyzed pathology in the K14-lnl/lnl mouse, as these mice accumulate GlcCer in all cell types in the brain (15) (Fig. 3B). The highest level of MAC2 staining was observed in the K14-lnl/lnl mouse, although previous observations (15) suggested more extensive MAC2 labeling in *Gba*$^{flox/flox}$;nestin-Cre mice; it should be noted that the K14-lnl/lnl mice used in the current study were backcrossed onto an outbred CD1 background, whereas in the original study mice were generated on a C57BL/6 background. The main differences between the three mice was that K14-lnl/lnl mice showed extensive MAC2 labeling throughout the brain, and most prominently in the brain stem, as also observed in mice injected with CBE (Table 2).

Use of the CBE model in determining pathological pathways and for testing therapeutic windows

We now took advantage of the accessibility and flexibility of inducing CBE in mice to further examine the temporal sequence of events leading to neuronal cell death and neuroinflammation, and to examine putative therapeutic windows upon cessation of CBE

treatment. We compared the time of appearance of degenerating neurons with the appearance of MAC2-positive microglia and GFAP-labeled astrocytes in mice treated with 37.5 mg/kg CBE. In contrast to *Gba*$^{flox/flox}$;nestin-Cre and K14-lnl/lnl mice, in which it is not possible to temporally distinguish between the appearance of MAC2-positive cells and neuronal loss (7), MAC2-positive cells were clearly visible on CBE day 18, when very few degenerating neurons (labeled with Fluoro-Jade C) were detectable (Fig. 4). The number of MAC2-positive cells increased significantly by day 25, although the number of Fluoro-Jade C-positive cells was still very low. A similar sequence was observed for GFAP-positive cells, indicating that microgliosis and astrogliosis precede neuronal loss.

Another advantage of the CBE model compared to genetic models is that CBE treatment can be stopped at various times, allowing examination of the reversibility of the pathology. We injected mice from a mixed genetic background (C57BL6/J and CBA) (18) with 100 mg/kg of CBE from post-natal day 15 for various lengths of time, followed by cessation of CBE treatment. The first group of mice was injected with CBE from days 15-35, with CBE treatment stopped in some mice on day 25 (Fig. 5). In the second group, mice were injected with CBE from days 15-48, with CBE treatment stopped in some mice on day 25, allowing a longer period of recovery after cessation of CBE treatment (Fig. 5). The third group of mice was injected with CBE for a longer period, from days 15-40, with CBE treatment stopped in some mice on day 30 (Fig. 6). The last group of mice was injected with CBE from days 15-74, with CBE treatment stopped in some mice on day 30 (Fig. 6).

In the first group, no effect on symptoms (*i.e.* body weight) was detected by day 24, but mice treated continuously with CBE lost considerable weight by day 35. Upon cessation of CBE treatment on day 24, mice gained weight similarly to control mice (Fig. 5A). Despite the lack of overt signs, a significant number of MAC2-positive cells were detected in CBE-treated mice on day 25, although considerably fewer MAC2-positive cells were seen on day

35 when CBE treatment was stopped on day 25 (Fig. 5B). Mice injected with CBE from days 15-25 displayed impaired motor behavior (Fig. 5C). Thus, the latency to fall was reduced by almost 1 min on the rotarod compared to the PBS-injected control group; in the hang wire test, mice injected with CBE normally fell off the wire within 10 seconds, due to difficulties using their hind limbs to hold on to the wire. The manual catwalk test demonstrated an increase in inter-limb distance of 0.5 cm in the group injected with CBE. Cessation of CBE treatment on day 25 led to no significant improvement in any of these parameters by day 35 or day 48, although, importantly, no deterioration in the behavioral parameters was detected (Fig. 5C).

The other two groups of mice were injected with CBE for longer period (days 15-30) and allowed to recover for a longer time (up to day 74) (Fig. 6). The additional time of injection with CBE had a deleterious effect, inasmuch as the mice did not gain body weight after cessation of CBE treatment on day 30 (Fig. 6A), and continued to lose weight, although a moderate reduction in the number of MAC2-positive cells (Fig. 6B) was observed. The number of MAC2-positive cells in cortical layer V increased almost 2-fold on day 74 in mice continuously injected with CBE; in this group, a number of mice died by day 74, which was accompanied by severe neuronal degeneration. No improvement in any behavioral parameters was detected (Fig. 6C), and even after cessation of CBE treatment, mice continued to deteriorate, exhibiting almost zero latency in the rotarod test and inability to hold on to the wire in the hang wire test, due to limb paralysis.

Discussion

In the current study, we have systematically characterized the use of CBE to induce GD in mice. The availability of a chemical inhibitor of GCase should, in principle, allow in-depth study of GD development in animal models, and should render GD more accessible to

experimental manipulation than almost all other LSDs, for which chemical inhibitors of the defective lysosomal enzymes are not readily available. Moreover, the enigmatic relationship between GD/nGD and PD is amenable to study using CBE. Although all the above statements appear axiomatic, the lack of methodical study of the dose, time of injection, levels of accumulation and comparison with genetic models of nGD has often led to skepticism regarding the suitability of CBE as a tool to induce GD/nGD, which the current study seeks to alleviate.

Unsurprisingly, we first showed that the amount of CBE injected into mice directly affects the course of development of GD pathology. However, injection of the same dose of CBE into 15-day-old mice resulted in far less severe pathology than in mice injected from day 8, suggesting that (i) the blood-brain barrier prevents CBE entry in older mice (30, 31), (ii) that CBE is less efficient in inhibiting GCase in older mice, (iii) that the brain is less sensitive to GlcCer accumulation in older mice, or (iv) that different levels of GlcCer synthesis in younger *vs.* older mice could affect the efficacy of CBE. Irrespective of the precise reason for this age-dependent change, the use of higher doses (Table 1) of CBE in older mice is thus justified.

The linear increase in levels of GlcCer and GlcSph accumulation upon increasing amounts of CBE is not surprising, but nevertheless supports the concept that disease severity is directly related to levels of substrate accumulation. Comparison of levels of GlcCer and GlcSph accumulation in mouse models compared to human patients is difficult, due to different methods of measurement, different units often used for quantification and large variability between different human samples, which might be related to parameters such as tissue storage post mortem (Table 4).

It should be stressed that a number of studies have injected relatively high amounts (100 mg/kg) of CBE into mice, such as those to examine the relationship between PD and

GD. While these studies have uncovered important findings, such as accumulation of α-synuclein, neurodegeneration and gliosis (32, 33), it should be noted that most GD patients have residual levels of GCase activity, and GD carriers with a higher susceptibility to develop PD have GCase activity in the range of ~50% of normal; we therefore suggest that although more time-consuming, a better way to study the GD/PD connection might be injection of low doses of CBE (<25 mg/kg) for longer periods of time, whereas the higher concentrations (>50 mg/kg) might be better suited for studying the acute forms of nGD. However, it should be noted that in general a larger variability in the phenotype of mice was observed when using lower doses of CBE, necessitating use of a larger group of mice, that should preferably be littermates with similar weights at the beginning of the injection period.

A previous concern using CBE was that it might not fully mimic the pathology observed in genetic models of GD or in human nGD patients. The reasons for this concern were three-fold. First, CBE might have off-target effects, *i.e.* inhibit other enzymes, which could influence pathology. Second, the penetration, or lack of penetration of CBE across the BBB might result in different patterns of brain pathology from those observed in genetic models. Third, induction of an LSD by chemical inhibition might miss changes that are due to the unfolded proteins often caused by amino-acid substitutions in GCase (34).

Although the first concern cannot be completely excluded, it is noticeable that many earlier studies reporting off-target effects of CBE in animal models used extremely high doses (sometimes as high as 300 mg/kg (35)). *In vitro* studies have shown that CBE can inhibit other enzymes such as GBA2, an extra-lysosomal GCase (36), but with lower affinity than GBA1 and at a much lower rate (37). CBE has also been shown to inhibit some retaining α-glucosidases (38) and lactase-phlorizin hydrolase (39). We conclude that although CBE might have minor off-target effects, few if any of these are likely to be responsible for the pathology observed, particularly using low levels of CBE. This does not alleviate the need to produce

better and more specific GCase inhibitors (40), but currently CBE is the cheapest and best commercially-available inhibitor. Finally, off-target effects of CBE could be further ruled out by treating *Gba*$^{flox/flox}$;nestin-Cre mice with CBE.

The second concern, that CBE might not mimic GD pathology, can also be alleviated by the current study, in which we show a remarkable overlap in gene profile changes after CBE injection, compared to *Gba*$^{flox/flox}$;nestin-Cre mice, and a rather similar pattern of brain pathology. This is particularly true when comparing the low dose of CBE with the *Gba*$^{flox/flox}$;nestin-Cre mice, although more severe brain pathology was seen in K14-lnl/lnl mice, which itself is not surprising based on the severity of the latter; presumably, a more severe pattern of pathology would be observed using a higher dose of CBE, although this is not something that we directly analyzed. It should also be noted that the regional pathology is somewhat similar to that in the few human brain samples that have been systematically analyzed. Thus, our current study negates to a large extent concerns that CBE does not cause similar pathological changes as in genetic models or in human patients.

The third concern, that CBE is a chemical inhibitor rather than mimicking the effect of unfolded, mutated proteins, is less tractable. However, mice treated with CBE do develop classical GD/nGD symptom, though whether a small subset of symptoms do not develop which might be induced by the unfolded protein response, cannot be excluded.

Having validated the use of CBE as a genuine tool to induce GD/nGD symptoms, we then further demonstrated the usefulness of this model by using it to tease out the temporal sequence of events that result in neuronal cell loss, astrogliosis and microgliosis; this is not possible using either the *Gba*$^{flox/flox}$;nestin-Cre or K14-lnl/lnl mice due to the rapid pathological progression in these mice. Moreover, cessation of CBE injection can be used to determine which symptoms are reversible, and which are not. Finally, a major advantage of the use of CBE is examination of the role of specific biochemical pathways in GD pathology,

as exemplified in our recent study showing a role for the Ripk pathway in nGD pathology (6), since CBE can be injected into mice defective in components of putative pathological pathways without the need for time-consuming crossing of mice. CBE can also be used in the study of other putative therapies, such as gene therapy (41), substrate reduction therapy (42), and for the study of biomarkers (28).

In summary, we have shown that, although it has some limitations, CBE provides an attractive and easy way to induce Gaucher disease in mice, which mimics to a large extent that which is observed in the two available mouse models that mimic neurological forms of GD.

Acknowledgments

This work was supported by an Investigator-Initiated Research (IIR) grant from Pfizer, by the Minerva Foundation and by the Children's Gaucher Research Fund. We thank Dr. Nicolas Panayotis for help in performing behavioral tests, data analysis and image preparation, Vladimir Kiss for help with microscopy, Tammar Joseph and Natalia Santos Ferreira for help in performing GCase activity assays, Giora Volpert for help with data analysis, Shifra Ben-Dor and Irit Orr for help with bioinformatics and Victoria Korzhova for help with immunohistochemistry. We thank Dr. Stefan Karlsson for providing the *Gba*$^{flox/flox}$;nestin-Cre mice and Dr. Simon N. Waddington (University College London) for providing K14-lnl/lnl mice. A.H. Futerman is the Joseph Meyerhoff Professor of Biochemistry at the Weizmann Institute of Science.

Author contributions

AV and HZ performed most of the experiments and helped with the writing of the manuscript. AM injected mice, performed behavioral tests and immunohistochemistry. ADK performed the gene array, CY and RE performed some of the immunohistochemistry and

BMK the mass spectrometry. AAR and GM performed some of the MAC2 immunostaining. AHM directed the mass spectrometry experiments. EBV helped with planning of the experiments. AHF obtained funding of the study, led the research and wrote the manuscript.

References

1. Futerman AH, and van Meer G. The cell biology of lysosomal storage disorders. *Nat Rev Mol Cell Biol* 2004; **5**: 554–565.

2. Hruska KS, LaMarca ME, Scott CR, *et al.* Gaucher disease: mutation and polymorphism spectrum in the glucocerebrosidase gene (GBA). *Hum Mutat* 2008; **29**: 567–583.

3. Vitner EB, Vardi A, Cox TM, *et al.* Emerging therapeutic targets for Gaucher disease. *Expert. Opin Ther Targets* 2014; **19**: 321–334.

4. Beutler E, and Grabowski GA. Gaucher disease. In Scriver,C., Beaudet,A., Sly,W., Valle,D. (eds), *The Metabolic and Molecular Bases of Inherited Disease*. New York: McGraw-Hill, 2001;3635–3668.

5. Sidransky E, Nalls M, and Aasly J. Multicenter Analysis of Glucocerebrosidase Mutations in Parkinson's Disease. *NEJM* 2009; **17**: 1651–1661.

6. Vitner EB, Salomon R, Farfel-Becker T, *et al.* RIPK3 as a potential therapeutic target for Gaucher's disease. *Nat Med* 2014; **20**: 204–208.

7. Farfel-Becker T, Vitner EB, Pressey SNR, *et al.* Spatial and temporal correlation between neuron loss and neuroinflammation in a mouse model of neuronopathic Gaucher disease. *Hum Mol Genet* 2011; **20**: 1375–1386.

8. Farfel-Becker T, Vitner EB, Kelly SL, *et al.* Neuronal accumulation of glucosylceramide in a mouse model of neuronopathic Gaucher disease leads to neurodegeneration. *Hum Mol Genet* 2014; **23**: 843–854.

9. Vitner EB, Dekel H, Zigdon H, *et al.* Altered expression and distribution of cathepsins in neuronopathic forms of Gaucher disease and in other sphingolipidoses. *Hum Mol Genet* 2010; **19**, 3583–3590.

10. Vitner EB, Farfel-Becker T, Eilam R, *et al.* Contribution of brain inflammation to neuronal cell death in neuronopathic forms of Gaucher's disease. *brain* 2012; **135**: 1724–1735.

11. Farfel-Becker T, Vitner E, Dekel H, *et al.* No evidence for activation of the unfolded protein response in neuronopathic models of Gaucher disease. *Hum Mol Genet* 2009; **18**: 1482–1488.

12. Lee H, Bae JS, and Jin HK. Defective self-renewal and differentiation of GBA-deficient neural stem cells can be restored by macrophage colony-ctimulating factor. *Mol Cells*

2015; **38**: 806–813.

13. Zigdon H, Meshcheriakova A, and Futerman AH. From sheep to mice to cells: tools for the study of the sphingolipidoses. *Biochim Biophys Acta* 2014; **1841(8);** 1189–1199.

14. Farfel-Becker T, Vitner EB, and Futerman AH. Animal models for Gaucher disease research. *Dis Model Mech* 2011; **4**: 746–752.

15. Enquist I B, Bianco Lo C, Ooka A, *et al.* Murine models of acute neuronopathic Gaucher disease. *PNAS* 2007; **104**: 17483–17488.

16. Kanfer JH, Legler G, Sullivan J, *et al.* (1975) The Gaucher mouse. *Biochem Biophys Res Commun* 1975; **67**: 85–90.

17. Stephens MC, Bernatsky A, Singh H, *et al.* Distribution of conduritol B epoxide in the animal model for Gaucher's disease (Gaucher mouse). *Biochim Biophys Acta* 1981; **672**: 29–32.

18. Feng G, Mellor RH, Bernstein M, *et al.* Imaging Neuronal Subsets in Transgenic Mice Expressing Multiple Spectral Variants of GFP. *Neuron* 2000; **28**: 41–51.

19. Meivar-Levy I, Horowitz M, and Futerman AH. Analysis of glucocerebrosidase activity using N-(1-[14C] hexanoyl)-D-erythroglucosylsphingosine demonstrates a correlation between levels of residual enzyme activity and the type of Gaucher disease. *biochem J.* 1994; **303**: 377–382.

20. Körschen HG, Yildiz Y, Raju DN, *et al.* The Non-lysosomal β-Glucosidase GBA2 Is a Non-integral Membrane-associated Protein at the Endoplasmic Reticulum (ER) and Golgi. *J Biol Chem* 2013; **288**: 3381–3393.

21. Bligh EG, and Dyer WJ. A rapid method of tatal lipid extraction and purification. *Can J Biochem Phys* 2011; **37**: 911–917.

22. Hulsen T, Vlieg J, and Alkema W. BioVenn - a web application for the comparison and visualization of biological lists using area-proportional Venn diagrams. *BMC Genomics* 2008; **9**: 488.

23. Alvarez AR, Klein A, Castro J, *et al.* Imatinib therapy blocks cerebellar apoptosis and improves neurological symptoms in a mouse model of Niemann-Pick type C disease. *FASEB J* 2008; **22**: 3617–3627.

24. Crawley JN. Behavioral Phenotyping Strategies for Mutant Mice. *Neuron* 2008; **57**: 809–818.

25. Sastry PS. (1985) Lipids of nervous tissue: Composition and metabolism. *Prog Lipid Res* 1985; **24**: 69–176.

26. Sun Y, Zhang W, Xu YH, *et al.* Substrate Compositional Variation with Tissue/Region and Gba1 Mutations in Mouse Models–Implications for Gaucher Disease. *PLoS ONE* 2013; **8**: e57560.

27. Valsecchi M, Mauri L, Casellato R, *et al.* Ceramide and sphingomyelin species of

fibroblasts and neurons in culture. *J Lipid Res* 2007; **48**: 417–424.

28. Zigdon H, Savidor A, Levin Y, *et al.* Identification of a Biomarker in Cerebrospinal Fluid for Neuronopathic Forms of Gaucher Disease. *PLoS ONE*, 2015; **10**: e0120194.

29. Mistry PK, Liu J, Sun L, *et al.* Glucocerebrosidase 2 gene deletion rescues type 1 Gaucher disease. *PNAS* 2014; **111**: 4934–4939.

30. Saunders NR, Dreifuss JJ, Dziegielewska KM, *et al.* The rights and wrongs of blood-brain barrier permeability studies: a walk through 100 years of history. *Front Neurosci* 2014; **8**: 404.

31. Saunders NR, Liddelow SA, and Dziegielewska KM. Barrier Mechanisms in the Developing Brain. *Front Pharmacol* 2012; **3**: 46.

32. Rocha EM, Smith GA, Park E, *et al.* Sustained Systemic Glucocerebrosidase Inhibition Induces Brain α-Synuclein Aggregation, Microglia and Complement C1q Activation in Mice. *Antioxid Redox Signal* 2015; **23**: 550–564.

33. Ginns EI, Mak SKK, Ko N, *et al.* Neuroinflammation and α-synuclein accumulation in response to glucocerebrosidase deficiency are accompanied by synaptic dysfunction. *Mol Genet Metab* 2014; **111**: 152–162.

34. Maor G, Rencus-Lazar S, Filocamo M, *et al.* Unfolded protein response in Gaucher disease: from human to Drosophila. *Orphanet J Rare Dis* 2013; **8**: 1–14.

35. Hara A, and Radin NS. Enzymic effects of β-glucosidase destruction in mice changes in glucuronidase levels. *Biochim Biophys Acta* 1979; **582**: 423–433.

36. Boot RG, Verhoek M, Donker-Koopman W, *et al.* Identification of the non-lysosomal Glucosylceramidase as beta- Glucosidase 2. *J Biol Chem* 2007; **282**: 1305–1312.

37. Ridley CM, Thur KE, Shanahan J, *et al.* Glucosidase 2 (GBA2) Activity and Imino Sugar Pharmacology. *J Biol Chem* 2013; **288**: 26052–26066.

38. Rempel BP, and Withers SG. Covalent inhibitors of glycosidases and their applications in biochemistry and biology. *Glycobiology*, 2008; **18**: 570–586.

39. Wacker H, Keller P, Falchetto R, *et al.* Location of the two catalytic sites in intestinal lactase-phlorizin hydrolase. Comparison with sucrase-isomaltase and with other glycosidases, the membrane anchor of lactase-phlorizin hydrolase. *J Biol Chem* 1992; **267**: 18744–18752.

40. Chao DHM, Kallemeijn WW, Marques ARA, *et al.* Visualization of Active Glucocerebrosidase in Rodent Brain with High Spatial Resolution following In Situ Labeling with Fluorescent Activity Based Probes. *PLoS ONE* 2015; **10**: e0138107.

41. Marshall J, McEachern KA, and Kyros J. Demonstration of feasibility of in vivo gene therapy for Gaucher disease using a chemically induced mouse model. *Mol Ther* 2002; **6**: 179–189.

42. Marshall J, Sun Y, Bangari D, *et al.* Evaluation of a novel substrate reduction therapy

with CNS access in mouse models of neuronopathic Gaucher disease. *Mol Genet Metab* 2015; **114**: S77–S78.

43. Adachi M, and Volk B. Gaucher disease in mice induced by conduritol-B-epoxide: morphologic features. *Arch Pathol Lab Med* 1977; **101**: 255–259.

44. Stephens MC, Bernatsky A, Burachinsky V, *et al.* The Gaucher mouse: differential action of conduritol B epoxide and reversibility of its effects. *J Neurochem* 1978; **30**: 1023–1027.

45. Hara A, and Radin NS. Destruction and resynthesis of mouse β-glucosidases. *Biochim Biophys Acta* 1979; **582**: 412–422.

46. Stephens MC, Bernatsky A, Legler G, *et al.* The Gaucher mouse: additional biochemical alterations. *J Neurochem* 1979; **32**: 969–972.

47. Datta SC, and Radin NS. Glucosylceramide and the level of the glucosidase-stimulating proteins. *Lipids* 1986; **21**: 702–709.

48. Datta SC, and Radin NS. Stimulation of liver growth and DNA synthesis by glucosylceramide. *Lipids* 1988; **23**: 508–510.

49. Datta SC, and Radin NS. Normalization of liver glucosylceramide levels in the 'Gaucher' mouse by phosphatidylserine injection. *Biochem Biophys Res Commun* 1988; **152**: 155–160.

50. Holleran WM, Ginns EI, Menon GK, *et al.* Consequences of beta-glucocerebrosidase deficiency in epidermis. Ultrastructure and permeability barrier alterations in Gaucher disease. *J Clin Invest* 1994; **93**: 1756–1764.

51. Marsh NL, Elias PM, and Holleran WM. Glucosylceramides stimulate murine epidermal hyperproliferation. *J Clin Invest* 1995; **95**: 2903–2909.

52. Marchell NL, Uchida Y, Brown BE, *et al.* Glucosylceramides Stimulate Mitogenesisin Aged Murine Epidermis. *J Invest Dermatol* 1998; **110**: 383–387.

53. Chan KW, Waire J, Simons B, *et al.* Measurement of lysosomal glucocerebrosidase activity in mouse liver using a fluorescence-activated cell sorter assay. *Anal Biochem* 2004; **334**: 227–233.

54. Xu YH, Reboulet R, Quinn B, *et al.* Dependence of reversibility and progression of mouse neuronopathic Gaucher disease on acid β-glucosidase residual activity levels. *Mol Genet Metab* 2008; **94**: 190–203.

55. Manning-Boğ AB, Schüle B, and Langston JW. Alpha-synuclein-glucocerebrosidase interactions in pharmacological Gaucher models: A biological link between Gaucher disease and parkinsonism. *NeuroToxicology* 2009; **30**: 1127–1132.

56. Xu YH, Sun Y, Ran H, *et al.* Accumulation and distribution of α-synuclein and ubiquitin in the CNS of Gaucher disease mouse models. *Mol Genet Metab* 2011; **102**: 436–447.

57. Pandey M, Tinch S, Inskeep V, *et al.* Glucosylceramide induced complement activation triggers inflammation in Gaucher disease (CCR5P.212). *J Immunol* 2015; **194**: 186.14–186.14.

58. Wong K, Sidransky E, Verma A, *et al.* Neuropathology provides clues to the pathophysiology of Gaucher disease. *Mol Genet Metab* 2004; **82**: 192–207.

59. Wong K. Neuropathological aspects of Gaucher disease. In Futerman,A.H., Zimran,A. (eds), *Gaucher disease* 2007; 225–248.

60. Nilsson O, and Svennerholm L. Accumulation of Glucosylceramide and Glucosylsphingosine (Psychosine) in Cerebrum and Cerebellum in Infantile and Juvenile Gaucher Disease. *J Neurochem* 1982; **39**: 709–718.

61. Conradi NG, Sourander P, Nilsson O, *et al.* Neuropathology of the Norrbottnian type of Gaucher disease. *Acta Neuropathol* 1984; **65**: 99–109.

62. Nilsson O, Grabowski GA, Ludman MD, *et al.* Glycosphingolipid studies of visceral tissues and brain from type 1 Gaucher disease variants. *Clin Genet* 1985; **27**: 443–450.

63. Kaye EM, Ullman MD, Wilson ER, *et al.* Type 2 and type 3 Gaucher disease: A morphological and biochemical study. *Ann Neurol.* 1986; **20**: 223–230.

64. Orvisky E, Ginns EI, and Sidransky E. Glucosylsphingosine accumulation in patients with Gaucher disease. *Am J Hum Genet* 1999; **65**: A427.

65. Orvisky E, Sidransky E, McKinney CE, *et al.* Glucosylsphingosine Accumulation in Mice and Patients with Type 2 Gaucher Disease Begins Early in Gestation. *Pediatr Res* 2000; **48**: 233–237.

66. Orvisky E, Park JK, LaMarca ME, *et al.* Glucosylsphingosine accumulation in tissues from patients with Gaucher disease: correlation with phenotype and genotype. *Mol Genet Metab* 2002; **76**: 262–270.

67. Lloyd-Evans E, Pelled D, Riebeling C, *et al.* Glucosylceramide and Glucosylsphingosine Modulate Calcium Mobilization from Brain Microsomes via Different Mechanisms. *J Biol Chem* 2003; **278**: 23594–23599.

68. Pelled D, Trajkovic-Bodennec S, Lloyd-Evans E, *et al.* Enhanced calcium release in the acute neuronopathic form of Gaucher disease. *Neurobiol Dis* 2005; **18**: 83–88.

Table 1. The use of CBE in GD research.

Mouse strain	CBE concentration *(mg/kg/day)*	Age[a] *(days)*	Duration of CBE treatment *(Days)*	Major findings	Ref.
C57/Bl	100	90	21	GlcCer levels elevated, and GCase activity reduced by 93% in brain, liver, and spleen. Activity of six other lysosomal hydrolases unaffected.	(16)
SWR/J	100	1	28	No Gaucher cells detected but spleen and liver showed irregular granules and fibrils. Neurons showed fibrils and tubular structures in the ER.	(43)
BALB/c	7.5,10	42-56	1	GCase activity was minimal the day after injection and returned to 40-50% by the 3rd/4th day.	(44)
BALB/c	10	42-56	42[b]	No elevation in GlcCer levels.	
BALB/c	10, 25,50,100	42-56	21-28	GCase activity decreased by ~68-88% using 10, 25 or 50 mg/kg and >90% using 100 mg/kg; similar levels of accumulation in brain and liver.	
BALB/c	100	42-56	21-28	Liver GCase activity gradually increased to ~50% of basal activity between day 4 and 8 after last injection and was 73% by day 12. Brain GCase activity increased more slowly.	
CF1	100	16	1	No detectable GCase activity in liver, spleen, brain, and kidney within 5 hours. Restoration of activity within 1 day (2 days in the case of brain) to ~80% of normal within 16 days. Reduction of aryl β-glucosidase activity (50%).	(45)
BALB/c	100	42-56	30	Several biochemical characteristics similar to human GD patients.	(46)
BALB/c	100	4	14		

CF-1	300	16	1	Effect on glucose-containing glycoprotein levels	(35)
CF-1	100	16	8	Increase in brain and liver size.	
C57BL/6	~20	28	1	[^{3}H]CBE rapidly distributed in the body but to a smaller extent in brain (~1/10 of systemic levels). Half-life of [^{3}H]CBE was ~7 hours and is not metabolized. >90% inhibition of GCase activity within 1-2 hours, with recovery of activity beginning after 4-12 hours.	(17)
CF-1	100	16	1	Rapid elevation in liver and brain saposin C. Increase persisted in both organs for at least seven days.	(47)
CF-1	80	16	1	Injection of emulsified GlcCer along with CBE caused rapid liver growth. Activity of thymidine kinase increased 46-73%, and activity of ornithine decarboxylase by 101%.	(48)
CF-1	80	16	1	Injection of emulsified GlcCer along with CBE caused rapid liver growth which was accelerated by phosphatidylserine.	(49)
hr/hr	375nmol[c]	56-84	1	brCBE[e] injection leads to <5% of normal epidermal GCase activity.	(50)
hr/hr	10µmol[c]	42-56	2[d]	Increased epidermal GlcCer localized largely to the basal, proliferative cell layer.	(51)
hr/hr	100µg[c]	30-720	1-2[d]	1.5- to 1.9-fold increase in epidermal DNA synthesis producing epidermal hyperplasia.	(52)
BALB/c	100	42-56	1	Used to demonstration feasibility of gene therapy; transduction of hepatocytes with human GCase resulted in normalization of Kupffer cell GlcCer levels.	(41)

BALB/c	100	20	1	New method for measuring GBA activity.	(53)
D409V, D409H, V394L[f]	100	5-15	10	Recapitulated the CNS phenotype of kn-9H mice GD mice. Neuronal degeneration was progressive in the 2 to 5 months after cessation of CBE injection.	(54)
C57BL/6	200	56	1	α-synuclein distribution was perturbed with accumulation in nigral cell bodies and astroglia.	(55)
D409V, D409H, V394L[f]	100	5	6 24/36	No α-synuclein accumulation. Shaking and paralysis after 6 injections. Hind limb paralysis and small amounts of α-synuclein accumulation.	(56)
C57BL/6	100	56	9	Markedly reduced striatal dopamine release and other changes in synaptic plasticity; altered microRNA profile and a reduction in post-synaptic density size.	(33)
Ripk3$^{-/-}$	25	56		Amelioration of nGD symptoms.	(6)
C5aR$^{-/-}$				No nGD signs.	(57)
C57BL/6	100	15	~30	Reduction in GPNMB levels in the cerebrospinal fluid upon cessation of CBE.	(28)
BDF1	100	21-28	28	Accumulation of insoluble α-synuclein aggregates in the substantia nigra; altered levels of proteins involved in the autophagy/lysosomal system, and widespread neuroinflammation, upregulation of complement C1q, abnormalities in synaptic, axonal transport and cytoskeletal proteins, and neurodegeneration.	(32)

[a] Age of mice at first injection; [b] CBE was injected every other day; [c] Topical injection; [d] 2 doses 5 hours apart; [e] Bromoconduritol B epoxide; [f] CBE was injected to all three strains

Table 2. Characterization and extent of microgliosis in nGD mouse models. Microgliosis was analyzed using MAC2 immunoreactivity at the end stage of the disease (CBE, 37.5 mg/kg from day 8 to 25; K14-lnl/lnl, day 14; *Gba*$^{flox/flox}$;nestin-Cre day 21). + indicates MAC2-immunoreactive microglia and - indicates no MAC2 immunoreactivity. n = 3.

	CBE	K14-lnl/lnl	*Gba*$^{flox/flox}$;nestin-Cre[a]
	General features		
Severity	Range of severity	Dies at ~2 weeks.	Dies at ~3 weeks
Affected organs	Systemic and brain	Systemic and brain	Brain
Brain region	*MAC2-immunoreactivity*		
Olfactory bulb	+	+	+
Cortical layer V[b]	+	+	+
Basal ganglia			
Globus pallidus (GP)[b]	+	+	+
Substantia nigra (SN)[b]	+	+	+
Hippocampus[c]	-	+	+
Hypothalamus	-	+	-
Thalamic nuclei[d]			
Reticular nucleus (Rt)	+	+	+
VPM/VPL	+	+	+
Midbrain			
Red nucleus	+	+	+
Periaqueductal gray (PAG)	-	+	-
Pons and medulla[b]			
Reticulotegmental nucleus of the pons (RtTg)	-	+	+
Pontine nucleus (Pn)	+	+	+
Facial nucleus (7N)	-	+	-
Vestibular nucleus (Ve)	-	+	+
Motor trigeminal nucleus (5N)	+	+	-

[a] Taken from Ref. 7; [b] Gliosis was documented in patients (4), (58, 59); [c] Gliosis was documented in patients in hippocampal layers CA2 to CA4 (58); [d] Gliosis was documented in patients in some thalamic nuclei (59).

Table 3. Top 10 up- and down- regulated genes in CBE-treated mice. Mice were injected with 25 mg/kg starting on day 8 for 10 days, and genes were analyzed in the cortex.

Gene symbol	Gene name	Fold-change (CBE *versus* PBS)	*p* value
	Top 10 up-regulated genes		
Ifit1	Interferon-induced protein with tetratricopeptide repeats 1	8.7	<0.001
Lilrb4	Leukocyte immunoglobulin-like receptor, subfamily B, member 4	8.2	<0.001
Oasl2	2'-5' Oligoadenylate synthetase-like 2	7.8	<0.001
Ccl5	Chemokine (C-C motif) ligand 5	6.5	<0.001
Usp18	Ubiquitin specific peptidase 18	6.4	<0.001
Cxcl10	Chemokine (C-X-C motif) ligand 10	6.2	<0.001
Ifi44	Interferon-induced protein 44	5.8	<0.001
Bst2	Bone marrow stromal cell antigen 2	5.1	<0.001
Ccl3	Chemokine (C-C motif) ligand 3	4.9	<0.001
Cybb	Cytochrome b-245, beta polypeptide	4.0	<0.001
	Top 10 down-regulated genes		
Agxt2l1	Alanine-glyoxylate aminotransferase 2-like 1	-1.91	<0.01
Snora44	Small nucleolar RNA, H/ACA box 44	-1.91	<0.01
Ptgds	Prostaglandin D2 synthase (brain)	-1.89	<0.05
Rn5s20	5S RNA 20	-1.73	<0.05
1700048 O20Rik	RIKEN cDNA 1700048O20 gene	-1.62	<0.01
Vmn2r15	Vomeronasal 2, receptor 15	-1.57	<0.01
Dcn	decorin	-1.56	<0.05
Pcdhb8	protocadherin beta 8	-1.56	<0.05
Mup3	major urinary protein	-1.56	<0.05
Fmod	fibromodulin	-1.54	<0.05

Table 4. GlcCer and GlcSph levels in human GD patient brain tissue.

GD type	GlcCer	GlcSph	Unit	Brain area	Assay and separation method[c]	Reference
2	140-530 (20-80x)[a]	3.8-8.8	µmol/kg wet weight	Cerebral cortex[b]	HPTLC	(60)
3	37-65 (7-13x)	0.8-4.6	µmol/kg wet weight	Cerebral cortex	HPTLC	
1[d]	38 (8x)	0.7	µmol/kg wet weight	Cerebral cortex	HPTLC	
3	59-1750 (4-109x)[e]	1.4- 6.3	µmol/kg wet weight	Cerebellar cortex[b]	HPTLC	(61)
1	36-92 (7-18x)	0.2-2.4	µmol/kg wet weight	Cerebral cortex[b]	HPTLC	(62)
2	1.9		nmol/mg protein	Temporal cortex[b]	HPLC	(63)
3	1.4		nmol/mg protein	Temporal cortex	HPLC	
2		9.8-935[e]	ng/mg protein	--	HPLC	(64)
3		8.9	ng/mg protein	--	HPLC	
1		0.34	ng/mg protein	--	HPLC	
2		304-437[g]	ng/mg protein	--	HPLC	**(65)**
3		14-32	ng/mg protein	--	HPLC	**(66)**
2		24-437	ng/mg protein	--	HPLC	
1		1	ng/mg protein	--	HPLC	
2	27.95 (14x)	4.88 (5x)	ng/mg protein	Cerebellum	2D-TLC[i]	(67)
2	8-36 (13x)	1.8-4.8	nmol/mg protein	Temporal lobe	2D-TLC	(68)
3	7-15 (5.5x)	0.2-1.2	nmol/mg protein	Temporal lobe	2D-TLC	

[a] Values in parenthesis indicate fold-change *vs.* controls; [b] Additional brain areas are given in the original paper; [c] High performance thin layer chromatography(HPLTC), two-dimensional thin-layer chromatography (2D-TLC); [d] Originally this sample was thought to be type 1 but further investigation suggest that it might be type 3; [e] 5 samples were analyzed and significant diversity was noted between them; [f] High performance liquid chromatography; [g] From fetal tissue.

Figure legends

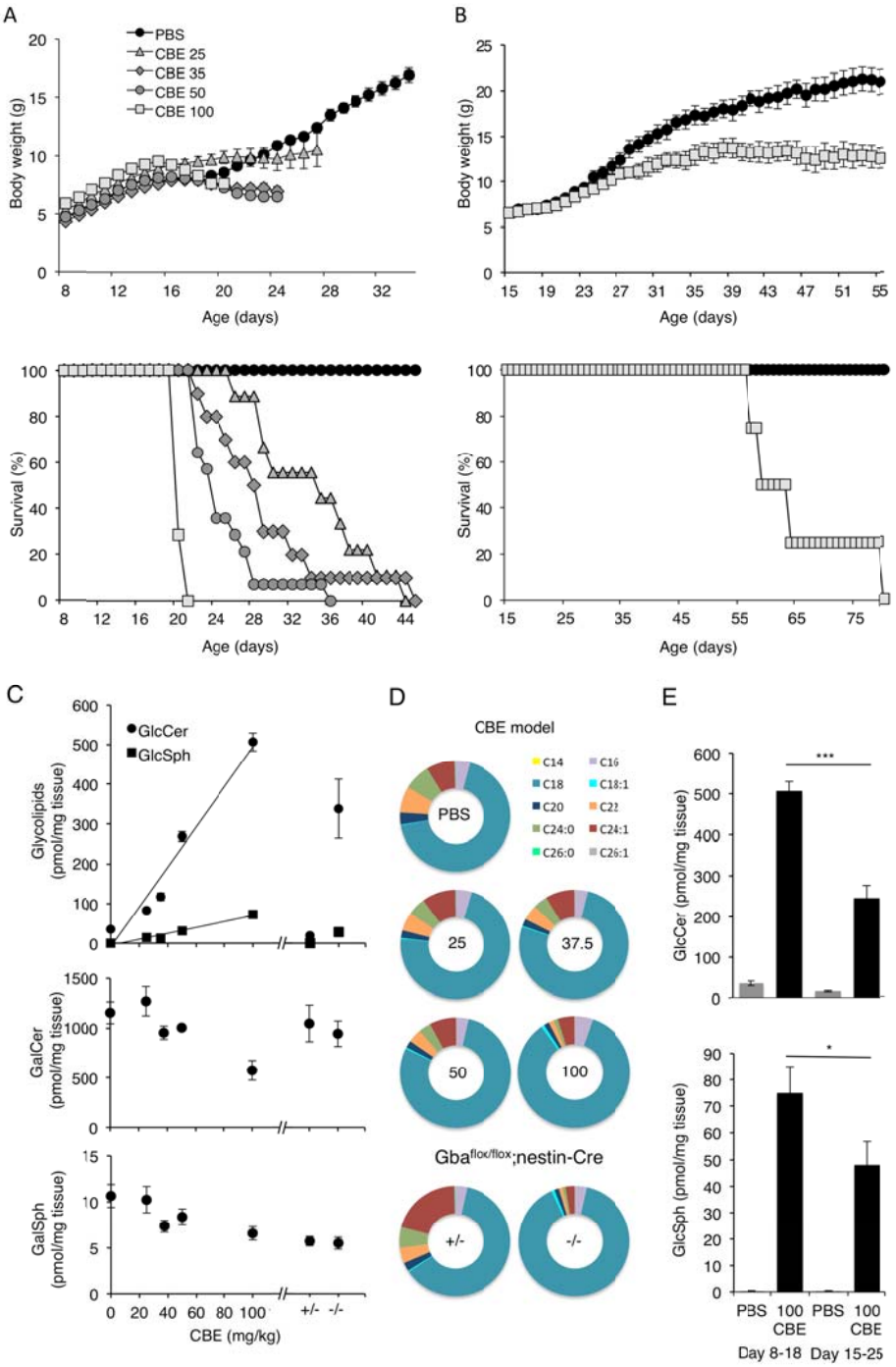

Figure 1. Life span and lipid levels in mice injected with CBE. (A) Body weight (upper panel) and Kaplan-Meier survival curve (lower panel) of C57BL/6 mice injected IP with PBS (n=15) or 25 (n=10), 37.5 (n=17), 50 (n=14) or 100 (n=7) mg/kg body weight CBE starting at 8 days of age. Values are means ± s.e.m. (B) Body weight (upper panel) and Kaplan-Meier

survival curve (lower panel) of C57BL/6 mice injected IP with PBS (n=4) or 100 mg/kg body weight CBE (n =4) starting at 15 days of age. Values are means ± s.e.m. (C) GlcCer, GlcSph (upper panel), GalCer (middle panel) and GalSph (lower panel) levels in brains of C57BL/6 mice injected IP with PBS or 25, 37.5, 50 or 100 mg/kg body weight CBE from post-natal days 8 to 18 (n=3). Lipid levels in 21-day old *Gba*$^{flox/WT}$;nestin-Cre mice (+/-) and *Gba*$^{flox/flox}$;nestin-Cre (-/-) mice (n=3) are also shown. Values are means ± s.e.m. (D) *N*-acyl chain composition of GlcCer. (E) GlcCer (upper panel) and GlcSph (lower panel) levels after injecting mice for 10 days with 100 mg/kg CBE starting either on post-natal days 8 or 15. * $p \leq 0.05$; ** $p \leq 0.01$; *** $p \leq 0.001$.

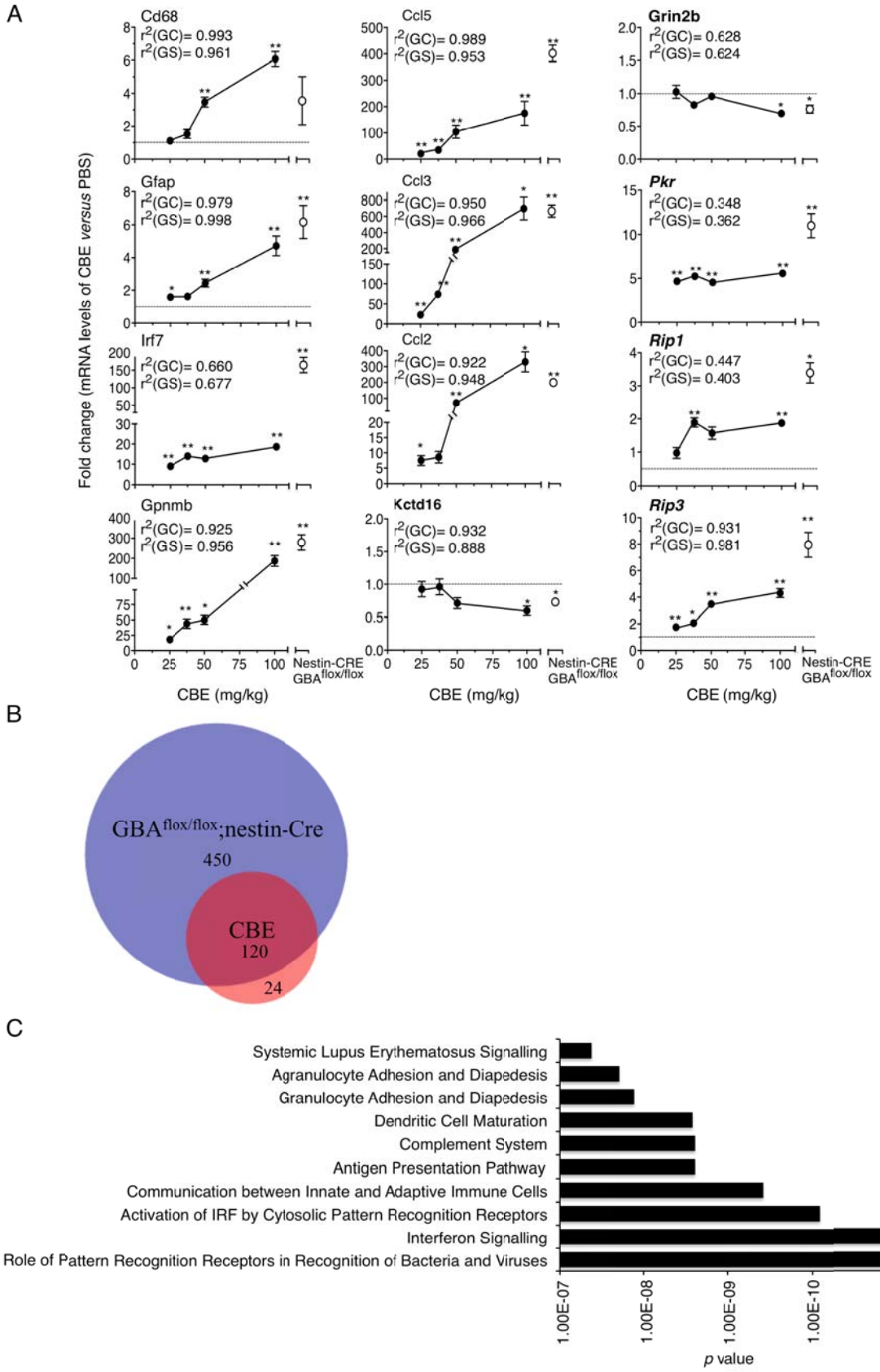

Figure 2. Gene expression in CBE-treated and in *Gba*$^{flox/flox}$;nestin-Cre mice. (A) mRNA levels of inflammatory genes, neuronal genes (bold) and genes associated with the Rip pathway (bold italics) were measured by qPCR on total mRNA extracted from the cortex of C57BL/6 mice injected IP with PBS or 25, 37.5, 50 or 100 mg/kg body weight CBE from day 8 to the end-stage of the disease (see Fig. 1A), and compared with levels of the same genes in 21-day-old *Gba*$^{flox/flox}$;nestin-Cre mice. Results are a ratio of CBE-treated mice *vs.* PBS-treated mice, and are means ± s.e.m. (n=2-3). * $p \leq 0.05$; ** $p \leq 0.01$. CT values were normalized to levels of TBP. Levels of each gene were correlated with levels of GlcCer (GC) or GlcSph (GS) measured for each dose of CBE (see Fig. 1C). (B) Venn diagram of the number of genes increased >2-fold in *Gba*$^{flox/flox}$;nestin-Cre mice (day 14, n=3) and >1.5-fold for C57/BL6 mice treated with 25 mg/kg CBE from days 8-18, n=3. Up-regulated genes in *Gba*$^{flox/flox}$;nestin-Cre mice are in purple and up-regulated genes in the CBE model are in pink. (C) Ten most significantly enriched pathways for up-regulated genes in C57/BL6 mice treated with 25 mg/kg CBE and in 14 day-old *Gba*$^{flox/flox}$;nestin-Cre mice. The plot shows the enrichment *p* values.

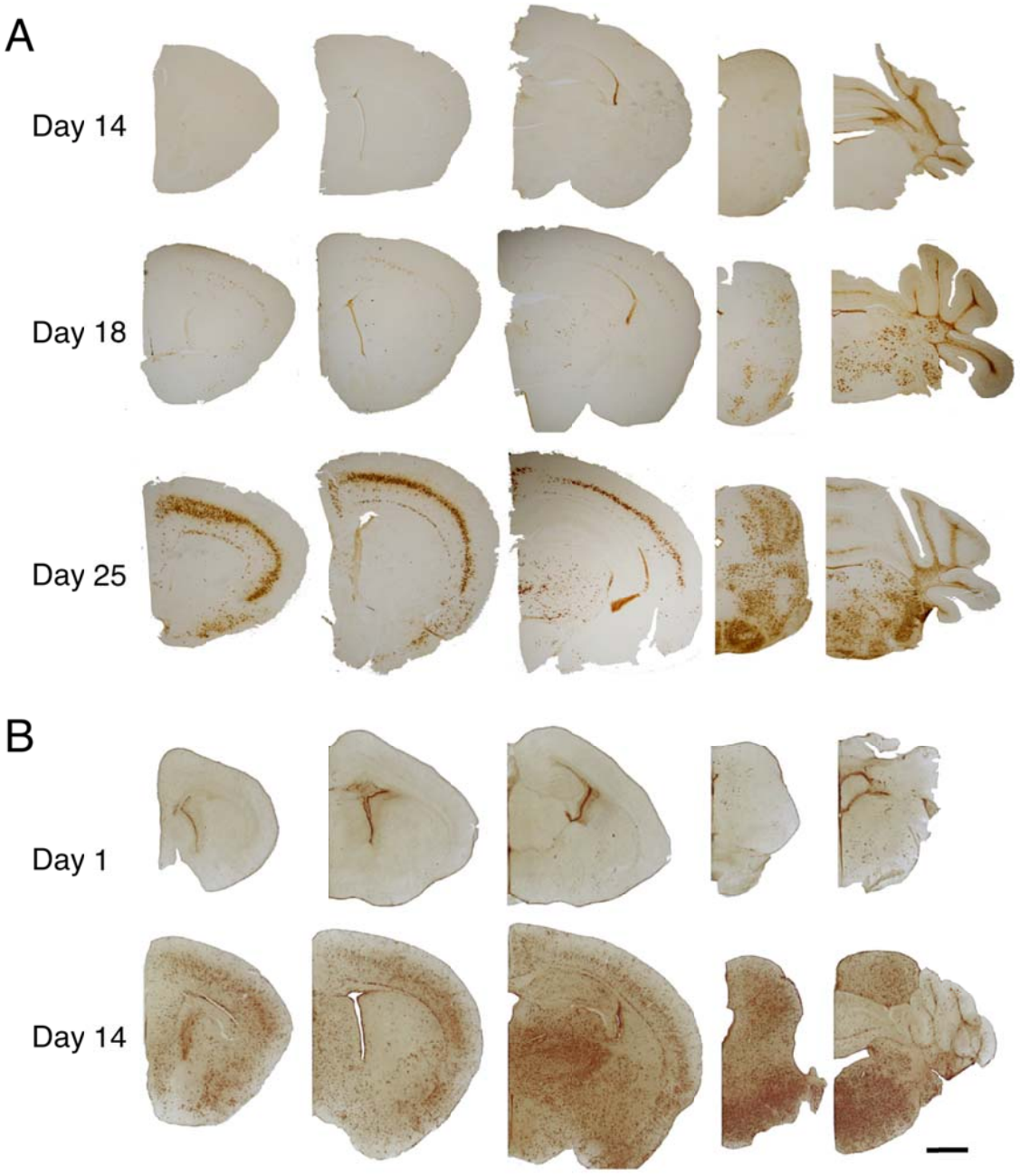

Figure 3. Microglia activation in CBE-treated and K14- lnl/lnl mice. Coronal sections labeled with an anti-MAC2 antibody of (A) 14-, 18- and 25-day-old C57BL/6 mice injected IP from day 8 with 37.5mg/kg CBE and (B) 1- and 14-day-old K14- lnl/lnl mice (scale bar, 1 mm). Results are representative of three biological replicates. No staining was observed in control brains.

Figure 4. **Inflammatory markers and neuronal loss in CBE-treated mice.** Coronal sections of cortical layer V in 14-, 18- and 25-day-old C57BL/6 mice injected IP with 37.5

mg/kg CBE from day 8, labeled with either Fluoro-Jade C (green) and DAPI (blue) (upper panel), MAC2 (red, middle panel) or GFAP (orange, lower panel). Arrows indicate labeled cells. Scale bar: 100 µm. Quantification of labeling is shown on the right, n=2-4; note that no Fluoro-Jade C- or MAC2-labeled cells could be detected in sections from mice injected with PBS. * p≤0.05; ** p≤0.01, *** p≤0.001. AU: arbitrary units.

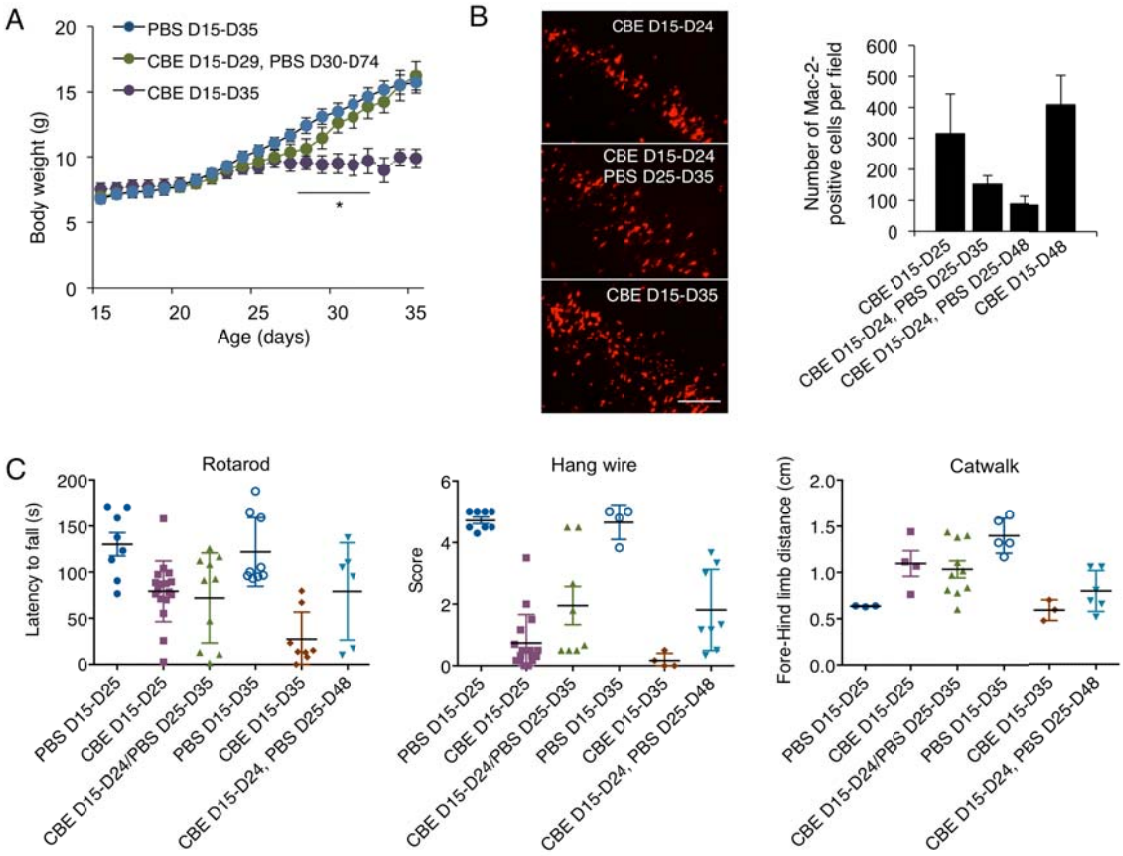

Figure 5. Pathological progression after cessation of CBE treatment at an early stage of the disease. (A) Body weight curves of mice injected with 100 mg/kg CBE from days 15-35, with CBE treatment stopped in some mice on day 25. (B) Quantification of the number of MAC2-positive cells in mice injected with 100 mg/kg CBE for different time periods. Data are means ± s.e.m. and were calculated from four consecutive slices for each sample. Scale bar: 100 µm. (C) Motor performance of mice injected with 100 mg/kg CBE from days 15-25 and from days 15-35, with CBE treatment stopped in some mice on day 25 and followed by 25-35 or 25-48 days of recovery. Each data point was obtained from an individual mouse. Data is means ± s.e.m, *p<0,05, **p<0,01, ***p<0,001. ns: not significant. Statistical analysis was performed using ANOVA followed by *post hoc* multiple comparison test (Tukey).

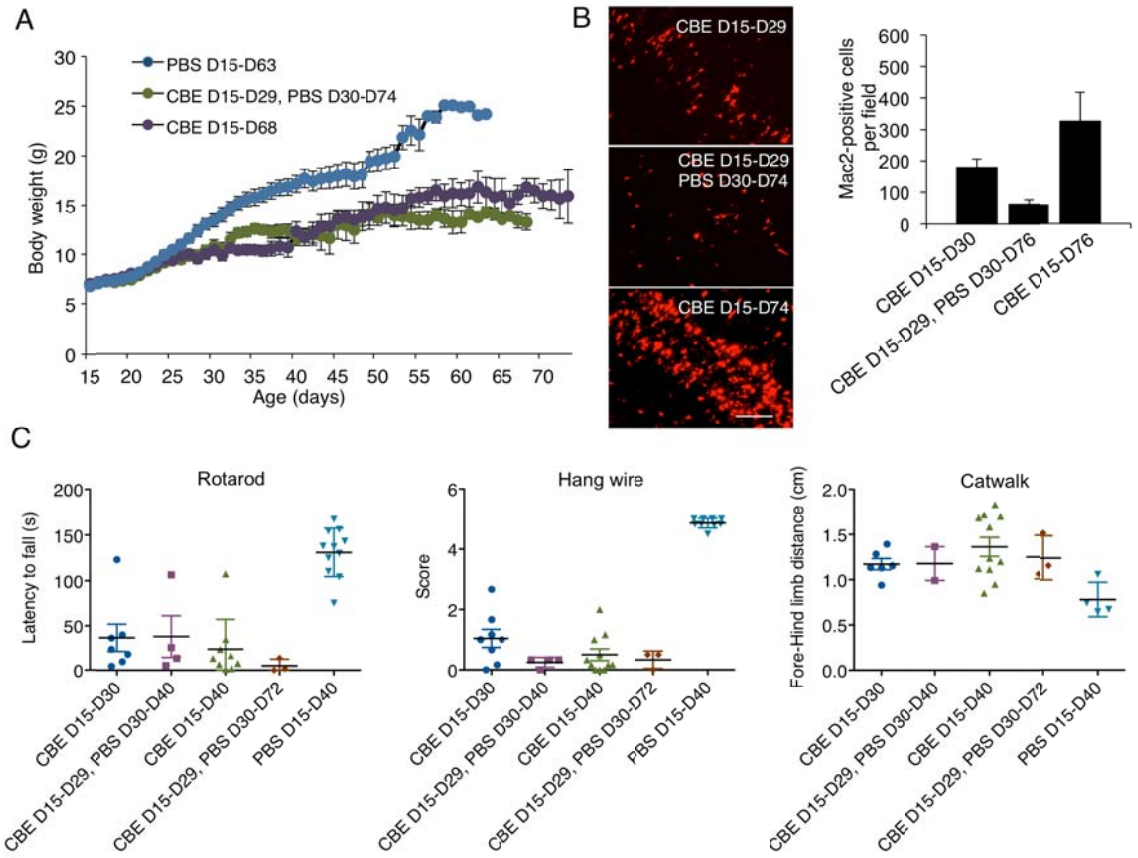

Figure 6. Pathological progression after cessation of CBE treatment at advanced stages of the disease. (A) Body weight curves of mice injected with 100 mg/kg CBE from days 15-74, with CBE treatment stopped in some mice on day 29. (B) Quantification of the number of MAC2-positive cells in mice injected with 100 mg/kg CBE for different time periods. Data are means ± s.e.m. and were calculated from four consecutive slices for each sample. Scale bar: 100 μm. (C) Motor performance of mice injected with 100 mg/kg CBE from days 15-30 and days 15-40, with CBE treatment stopped in some mice on day 29 followed by 30-40 or 30-72 days of recovery. Each data point was obtained from an individual mouse. Data is means ± s.e.m, *p<0,05, **p<0,01, ***p<0,001. ns: not significant. Statistical analysis was performed using ANOVA followed by *post hoc* multiple comparison test (Tukey).